Chemo-spectrophotometric evolution of spiral galaxies: V. Properties of galactic discs at high redshift

Samuel Boissier, N. Prantzos

Mon. Not. R. Astron. Soc. **325,** 321–334 (2001)

Chemo-spectrophotometric evolution of spiral galaxies – V. Properties of galactic discs at high redshift

S. Boissier and N. Prantzos★

Institut d'Astrophysique de Paris, 98bis, Bd. Arago, 75014 Paris, France

Accepted 2001 February 15. Received 2001 February 5; in original form 2000 June 22

ABSTRACT

We explore the implications for the high-redshift universe of 'state-of-the-art' models for the chemical and spectrophotometric evolution of spiral galaxies. The models are based on simple 'scaling relations' for discs, obtained in the framework of cold dark matter models for galaxy formation, and were 'calibrated' so as to reproduce the properties of the Milky Way and of nearby discs (at redshift $z \sim 0$). In this paper, we compare the predictions of our 'hybrid' approach to galaxy evolution to observations at moderate and high redshift. We find that the models are in fairly good agreement with observations up to $z \sim 1$, while some problems appear at higher redshift (provided there is no selection bias in the data); these discrepancies may suggest that galaxy mergers (not considered in this work) played a non-negligible role at $z > 1$. We also predict the existence of a 'universal' correlation between abundance gradients and disc scalelengths, independent of redshift.

Key words: galaxies: abundances – galaxies: evolution – galaxies: general – galaxies: photometry – galaxies: spiral.

1 INTRODUCTION

Important progress has been made in the past few years in our understanding of galaxy evolution, mainly because of the number and the quality of observations of galaxies at intermediate redshifts (up to $z \sim 1$). Observations of ground-based telescopes, combined with results from the *Hubble Space Telescope* (*HST*), provided photometric and kinematic data on the size, luminosity and rotational velocity of galactic discs as a function of redshift (Schade et al. 1996; Vogt et al. 1997; Lilly et al. 1998; Roche et al. 1998; Simard et al. 1999). Although the question of various selection effects is not settled yet, these data allow us, in principle, to probe the evolution of normal galaxies and to test theories of galaxy formation.

Several attempts have been made to interpret these data in the framework of currently popular models of hierarchical growth of structure in the Universe. Combined with simple assumptions about angular momentum conservation, such models lead to simple scaling relations as a function of redshift and may successfully reproduce some of the aforementioned high-redshift data (Mo, Mao & White 1998; van den Bosch 1998; Steinmetz & Navarro 1999; Avila-Reese & Firmani 2000; Firmani & Avila-Reese 2000). This 'forwards' approach infers the structural properties of discs from those of the corresponding dark matter haloes and does not consider in detail the driving force of galaxy evolution, namely the transformation of gas to stars; for that reason, assumptions have to be made about the variation of the mass-to-light ratio and the colours of a disc as function of its mass and redshift, while the associated chemical evolution is, in general, ignored.

On the other hand, several studies (Ferrini et al. 1994; Prantzos & Aubert 1995; Chiappini, Matteucci & Gratton 1997; Boissier & Prantzos 1999) focused mainly on the properties of local discs, for which a large body of observational data is available. In those studies, the observed chemical and photometric profiles of discs are used to constrain the radial variation of the star formation rate (SFR) and of the infall rate. These multizone models naturally lead to a relation between luminosity and size (i.e. exponential scalelength) of discs. The fact that the Milky Way is a typical disc galaxy helps to 'calibrate' such models, but there is no simple prescription as to how to extend them to other discs.

In principle, one can utilize a 'backwards' approach and try to infer the properties of high-redshift discs from the histories of the models that reproduce well the local disc population. Such an approach has been adopted in Cayon, Silk & Charlot (1996), Bouwens et al. (1997), Prantzos & Silk (1998) and Bouwens & Silk (2001). In the latter work, a comparison is made between simplified versions of the 'forward' and 'backwards' approaches.

A kind of 'hybrid' approach is adopted in Jimenez et al. (1998): they relate the disc surface density profile to the properties of the associated dark matter halo, while they adopt radially varying SFR and infall time-scales such as to reproduce in detail current profiles of the Milky Way disc. While Jimenez et al. (1998) applied their model to the study of low surface brightness galaxies, we developed a modified and more detailed version of this 'hybrid'

★E-mail: prantzos@iap.fr

model and applied it extensively to the study of local discs. In a series of papers (Boissier & Prantzos 1999, 2000; Boissier et al. 2001; Prantzos & Boissier 2000a) we showed that this model can readily reproduce a large number of local disc properties: Tully–Fisher relations in various wavelength bands, colour–colour and colour–magnitude relations, gas fractions versus magnitudes and colours, abundances versus local and integrated properties, abundance gradients, as well as integrated spectra as a function of the rotational velocity of a galaxy. A crucial ingredient for the success of the model is the assumption that the infall rate scales with mass of the galaxy, i.e. massive discs form the bulk of their stars earlier than low-mass ones.

Stimulated by the success of this 'hybrid' model in reproducing properties of the local disc population, we explore in this work its implications for the high-redshift Universe, comparing its predictions to data of recent surveys. The plan of the paper is as follows. In Section 2, we present the models that were developed in the previous papers of this series in order to match the properties of the Milky Way and of nearby spirals; we also present the adopted probability distributions of the two main parameters of our models, namely the disc rotational velocity V_C and its spin parameter λ. The predictions for the evolution of spirals, deduced from those models, is shown in Section 3. In Section 4 we compare the results of models with observations up to $z = 1$. In Section 5, we explore the implications at higher redshifts and we compare our results with scalelength distributions observed up to $z = 3.5$; we also predict that abundance gradients and scalelengths should present at all redshifts the same correlation as the one observed locally. The conclusions of our 'backwards' approach for the exploration of the high-redshift Universe of disc galaxies are summarized in Section 6.

2 MODELS AND RESULTS FOR NEARBY DISCS

In this section we briefly describe the main ingredients and the underlying assumptions of our model for the chemical and spectrophotometric evolution of spiral galaxies. The model has been 'calibrated' in order to reproduce the properties of the Milky Way disc (Section 2.1), then extended to other spirals with the help of simple scaling relations that allow us to reproduce fairly well most of the observed properties of nearby spirals (Section 2.2). In Section 2.3 we present the adopted distribution functions concerning the two main parameters of our disc models, namely the rotational velocity V_C and the spin parameter λ.

2.1 The Milky Way model

The model for the Milky Way disc is presented in detail in Boissier & Prantzos (1999, hereafter Paper I). The galactic disc is simulated as an ensemble of concentric, independently evolving rings, gradually built up by infall of primordial composition. The chemical evolution of each zone is followed by solving the appropriate set of integro-differential equations (Tinsley 1980), without the instantaneous recycling approximation. Stellar yields are from Woosley & Weaver (1995) for massive stars and Renzini & Voli (1981) for intermediate mass stars. Fe-producing SNIa are included, their rate being calculated with the prescription of Matteucci & Greggio (1986). The adopted stellar initial mass function (IMF) is a multi-slope power law between 0.1 and 100 $M_\odot$ from the work of Kroupa, Tout & Gilmore (1993).

The spectrophotometric evolution is followed in a self-consistent way, i.e. with the SFR $\Psi(t)$ and metallicity $Z(t)$ of each zone determined by the chemical evolution, and the same IMF. The stellar lifetimes, evolutionary tracks and spectra are metallicity-dependent; the first two are from the Geneva library (Schaller et al. 1992; Charbonnel et al. 1996) and the latter from Lejeune, Cuisinier & Busser (1997). Dust absorption is included according to the prescriptions of Guiderdoni et al. (1998) and assuming a 'sandwich' configuration for the stars and dust layers (Calzetti, Kinney & Starchi-Bergmann 1994).

The star formation rate (SFR) is locally given by a Schmidt-type law, i.e. proportional to some power of the gas surface density Σ_g, and varies with galactocentric radius R as

$$\Psi(t,R) = \alpha \Sigma_g(t,R)^{1.5} V(R) R^{-1}, \quad (1)$$

where $V(R)$ is the circular velocity at radius R. This radial dependence of the SFR is suggested by the theory of star formation induced by density waves in spiral galaxies (e.g. Wyse & Silk 1989). The efficiency α of the SFR (equation 1) is fixed by the requirement that the observed local gas fraction $\sigma_g(R_0 = 8\,\mathrm{kpc}) \sim 0.2$ is reproduced at $T = 13.5\,\mathrm{Gyr}$.

The infall rate is assumed to be exponentially decreasing in time with a characteristic time τ. In the solar neighbourhood we adopt $\tau = 7\,\mathrm{Gyr}$ in order to reproduce the local G-dwarf metallicity distribution (Paper I). In order to mimic the 'inside out' formation of the disc, τ is assumed to be shorter in the inner zones and larger in the outer ones.

The really 'free' parameters of the model are the radial dependence of the infall time-scale $\tau(R)$ and of the SFR $\Psi(R)$. It turns out that the number of observables explained by the model is much larger than the number of free parameters. In particular the model reproduces present day 'global' properties (gas, O/H, SFR, and supernova rates), as well as the current disc luminosities in various wavelength bands and the corresponding radial profiles of gas, stars, SFR and metal abundances; moreover, the adopted inside-out star-forming scheme leads to a scalelength of $\sim$4 kpc in the B band and $\sim$2.6 kpc in the K band, in agreement with observations (see Paper I).

2.2 Extension to other disc galaxies

In order to extend the model to other disc galaxies we adopt the 'scaling properties' derived by Mo et al. (1998, hereafter MMW98) in the framework of the cold dark matter (CDM) scenario for galaxy formation. According to this scenario, primordial density fluctuations give rise to haloes of non-baryonic dark matter of mass M, within which baryonic gas condenses later and forms discs of maximum circular velocity V_C. It turns out that disc profiles can be expressed in terms of only two parameters: rotational velocity V_C (measuring the mass of the halo and, by assuming a constant halo/disc mass ratio, also the mass of the disc) and spin parameter λ (measuring the specific angular momentum of the halo). If all discs are assumed to start forming their stars at the same time, the profile of a given disc can be expressed in terms of the one of our Galaxy (the parameters of which are designated hereafter by index G):

$$\frac{R_d}{R_{dG}} = \frac{\lambda}{\lambda_G} \frac{V_C}{V_{CG}} \quad (2)$$

and

$$\frac{\Sigma_0}{\Sigma_{0G}} = \left(\frac{\lambda}{\lambda_G}\right)^{-2} \frac{V_C}{V_{CG}}. \quad (3)$$

Equations (2) and (3) allow us to describe the mass profile of a

galactic disc in terms of the one of our Galaxy and of two parameters: V_C and λ. The range of observed values for the former parameter is 80–360 km s^{-1} (with $V_{CG} = 220$ km s^{-1}), whereas for the latter numerical simulations give values in the 0.01–0.15 range (with $\lambda_G \sim 0.03$–0.06). Larger values of V_C correspond to more massive discs and larger values of λ to more extended ones. Although it is not clear yet whether V_C and λ are independent quantities, we treated them as such and we constructed a grid of 25 models characterized by $80 < V_C < 360$ km s^{-1} and $1/3 < \lambda/\lambda_G < 3$.

As discussed in Boissier & Prantzos (2000, hereafter Paper II) the resulting disc radii and central surface brightness are in excellent agreement with observations, except for the smallest values of λ ($\sim 1/3\lambda_G$); this 'unphysical' value leads to galaxies resembling bulges or ellipticals, rather than discs.

The two main ingredients of the model, namely the star formation rate $\Psi(R)$ and the infall time-scale $\tau(R)$, are affected by the adopted scaling of disc properties in the following way.

(i) For the SFR we adopt the prescription of equation (1), with the same efficiency α as in the case of the Milky Way (i.e. the SFR is not a free parameter of the model). In order to have an accurate evaluation of $V(R)$ across the disc, we calculate it as the sum of the contributions of the disc and of the dark halo, the latter having the density profile of a non-singular isothermal sphere (see Paper II).

(ii) The infall time-scale is assumed to decrease with both surface density (i.e. the denser inner zones are formed more rapidly) and the mass of a galaxy, i.e. $\tau[M_d, \Sigma(R)]$. In both cases it is the larger gravitational potential that induces a more rapid infall. The radial dependence of τ on $\Sigma(R)$ is calibrated on the Milky Way, while the mass dependence of τ is adjusted so as to reproduce the properties of the galactic discs.

This model, 'calibrated' on the Milky Way and having as main parameter the infall dependance on galaxy mass, reproduces fairly well a very large number of properties of spiral galaxies at low redshift (Paper II): Tully–Fisher relations in various wavelength bands, colour–colour and colour–magnitude relations, gas fractions versus magnitudes and colours, abundances versus local and integrated properties, as well as spectra for different galactic rotational velocities. The main assumption of the model is that infall on to massive discs occurred earlier than infall on to low-mass galaxies. More recently, in Paper IV (Boissier et al. 2001), we used a homogeneous set of observational data (a subset of the data presented in Boselli et al. 2000) in order to test this hypothesis. We determined the gas fraction $\sigma_G = M_{GAS}/M_{TOT}$ and the star formation efficiency ϵ in a large number of 'normal' spirals as a function of circular velocity V_C. We found that ϵ is independent of V_C while σ_G decreases with V_C. Taken at face value, those findings imply that low-mass discs did not have access to their gas reservoir as early as massive ones, otherwise they should have already turned most of their gas into stars (because their current star formation efficiency is similar to that of massive discs, and we assume that this has always been the case). This crucial finding justifies the assumptions we made concerning the form of the infall.

We notice that in another recent work, Brinchmann & Ellis (2000) found that the total stellar mass density in massive galaxies is constant over the redshift range $0.2 < z < 1$. This implies that the stellar content of these galaxies must have formed at higher redshifts, which is in qualitative agreement with our assumptions.

Finally, it is worth noting that the properties of abundance and colour gradients among local spirals are readily reproduced by the generalization of the Milky Way model and the assumed radial dependence of the SFR and infall time-scales (Prantzos & Boissier 2000a, herefter Paper III).

2.3 Distributions of the parameters V_C and λ

Our models presented in Section 2.2 simulate the evolution of individual disc galaxies, characterized by V_C and λ. In order to treat the evolution of the disc population, we need to make some assumptions about the probability distributions of the relevant parameters. In this paper we assume that the distributions $F_\lambda(\lambda)$ and $F_V(V_C)$ are independent and do not evolve in time. We adopt the velocity distribution suggested in Gonzalez et al. (2000):

$$F_V(V)\,\mathrm{d}V = \tilde{\Psi}_* \left(\frac{V}{V_*}\right)^{\beta} \exp\left[-\left(\frac{V}{V_*}\right)^{n}\right] \frac{\mathrm{d}V}{V_*}. \quad (4)$$

The parameters Ψ_*, V_*, β and n are determined in Gonzalez et al. (2000) on the basis of observed Tully–Fisher relationships and luminosity (Schechter-type) functions. We adopt here the set of parameters from their table 4 (fifth row, LCRS–Courteau data) corresponding to the velocity interval covered by our models. By construction, the distribution of equation (4) is normalized to the local luminosity function for spirals.

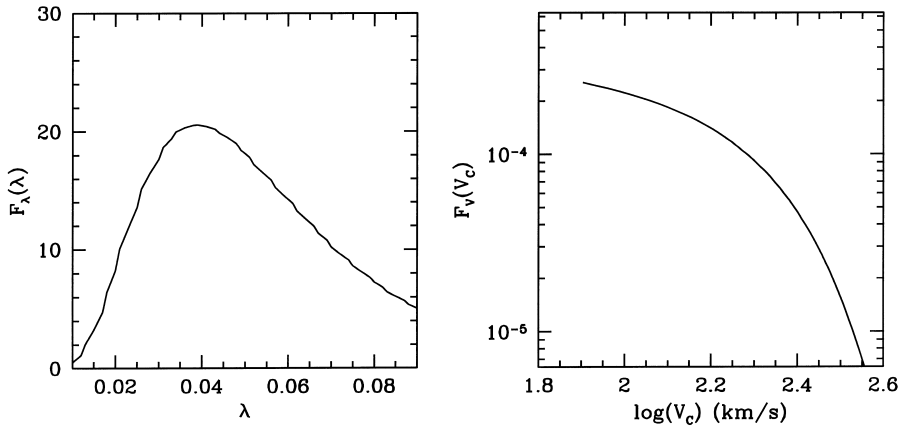

Figure 1. Adopted distributions of the two parameters characterizing our models of disc galaxies: spin parameter λ (left) and circular velocity V_C (right). The λ distribution is normalized to $\int F(\lambda)\,\mathrm{d}\lambda = 1$, while the V_C distribution is normalized to the local luminosity function in Gonzalez et al. (2000). See text (Section 2.3) for details.

The distribution of the spin parameter is given by

$$F_\lambda(\lambda)\,\mathrm{d}\lambda = \frac{1}{\sqrt{2\pi}\sigma_\lambda}\exp\left[-\frac{\ln^2(\lambda/\bar{\lambda})}{2\sigma_\lambda^2}\right]\frac{\mathrm{d}\lambda}{\lambda}, \quad (5)$$

with $\bar{\lambda} = 0.05$ and $\sigma_\lambda = 0.5$, according to numerical simulations (see e.g. MMW98). The distribution $F_\lambda(\lambda)$ is normalized to unity.

Distributions $F_\lambda(\lambda)$ and $F_V(V_C)$ are shown in Fig. 1. Low-mass discs are more numerous than high-mass ones, while the spin parameter distribution favours discs with intermediate λ values. Notice that in this work we study discs with $V_C > 80\,\mathrm{km\,s^{-1}}$ and $\lambda < 0.1$, because discs with larger λ values lead to low surface brightness galaxies (e.g. Jimenez et al. 1998), which will be the subject of a forthcoming paper (Boissier & Prantzos, in preparation).

In the following, we assume that the number of discs with velocity V_C and spin parameter λ is $\mathrm{d}N = F_V(V_C)F_\lambda(\lambda)\,\mathrm{d}V_C\,\mathrm{d}\lambda$; we compute then the distribution $\phi(Q)$ of various quantities Q (magnitude, radius, etc), defined by $\mathrm{d}N = \phi(Q)\,\mathrm{d}Q$.

We make the assumption that the circular velocity and spin parameter of a galaxy are determined at its formation and do not evolve in time. As the distributions $F_V(V)$ and $F_\lambda(\lambda)$ are always the same, any evolution in $\phi(Q)$ results from changes in intrinsic properties of individual galaxies, according to our models. It is clear that this assumption is an (important) oversimplification, because some spirals may merge (into e.g. ellipticals), modifying $F_V(V)$. The history of spirals that we present concerns only fairly isolated discs, that have not suffered major merger episodes.

3 MODEL PREDICTIONS FOR THE EVOLUTION OF SPIRALS

In Fig. 2 we present the results of our models concerning the evolution of the distribution functions of various quantities: disc scalelengths R_B in the B band (top left), central surface brightness $\mu_0(B)$ in the B band (top right), B magnitude M_B (middle left), colour index $(U-V)_{AB}$ (middle right), average oxygen abundance in the gas [O/H] (bottom left) and star formation rate ψ (bottom right). The corresponding distributions are shown at various redshifts, starting at $z = 4.2$ (*dashed curves*) and ending at $z = 0$ (*solid curves*). A cosmological model with matter density $\Omega_M = 0.3$, $\Omega_\Lambda = 0.7$ and $H_0 = 65\,\mathrm{km\,s^{-1}\,Mpc^{-1}}$ is adopted throughout this work.

The comparison of our results with observations of local spirals has been made in previous papers (Papers II and III). Here we comment on the evolution of the distribution functions $\phi(Q)$ that we obtain. As can be seen from Fig. 2, there has been a small but steady evolution in the distribution of R_B, with all discs becoming progressively larger. Disc scalelengths span today the range 0.8–11 kpc, compared with 0.3–6 kpc at $z \sim 4$. This is a result of the inside-out star formation scheme adopted in our models (see Section 2.1 and Paper II). The most probable value has increased only slightly between $z = 4.2$ and $z = 0$, from $\sim$1 kpc to $\sim$1.5 kpc.

The central surface brightness $\mu_0(B)$ is found to span a rather narrow range of values today (20–22.5 mag arcsec^{-2}). Notice, however, that our models were developed to reproduce properties of high surface brightness discs, while low surface brightness ones [i.e. with $\mu_0(B) > 22.5\,\mathrm{mag\,arcsec^{-2}}$] could be obtained by larger values of the spin parameter λ (e.g. Jimenez et al. 1998). We find that, at higher redshifts spirals had on average higher central surface brightness [lower $\mu_0(B)$], spanning a much broader range of values. This is a result of the fact that, in our scheme, massive and compact discs evolved quite rapidly and thus developed very high central surface brightness early on; low-mass and extended discs evolved slowly, starting from quite low values of central surface brightness and developing progresssively brighter central regions.

The M_B distribution function was also broader at early times, but massive and bright discs became progresssively fainter, while low-mass ones became increasingly brighter. The most probable M_B value shifted by ~ -3 mag in the past $\sim$10 Gyr.

The colour distribution function $\phi(U-V)$ shows considerable evolution in both its shape and average value. As time goes on, galaxies become (obviously) redder, while the increasing difference in effective ages between massive discs (formed early on) and low-mass ones (formed much later) contributes to broaden the $\phi(U-V)$ function.

The average metallicity is defined as the amount of oxygen in the gas divided by the gaseous mass of the disc. It increases steadily with time in all discs. At early times, massive discs have already developed relatively high O/H values, while low-mass ones are essentially unevolved; the $\phi(O/H)$ distribution is then quite broad, as in the case of $\phi(M_B)$. At late times, massive discs show little evolution while the metallicity of low-mass ones increases rapidly, and the $\phi(O/H)$ distribution becomes narrower.

Similar arguments hold for the distribution of the SFR $\phi(\Psi)$, which spans a large range of values at early times, from $10^{-3}\,\mathrm{M_\odot\,yr^{-1}}$ to $60\,\mathrm{M_\odot\,yr^{-1}}$. At late times, SFR values range from $10^{-1}\,\mathrm{M_\odot\,yr^{-1}}$ to $10\,\mathrm{M_\odot\,yr^{-1}}$, with an average around $1\,\mathrm{M_\odot\,yr^{-1}}$.

An interesting consequence of our models is that the average Fe/O ratio becomes slightly higher than solar at $z \sim 0$, because the rate of SNIa (major Fe producers) is such that their contribution slightly exceeds the one of O from SNII.

In summary: the distributions of $\mu_0(B)$, M_B, O/H and Ψ become narrower with time and shift to higher average values. Both effects result from the rapid late evolution of the numerous low-mass discs; because of this late evolution, the large differences created initially by the rapid early evolution of massive discs are reduced at late times. The distribution of R_B keeps its overall shape, but its peak value slightly increases. Finally, the distribution of $(U-V)$ is the only one that broadens with time, because of the increasing difference between the effective ages of massive and low-mass discs.

The results of Fig. 2 are presented in Fig. 3 in a different form. The evolution of the average values of R_B, $\mu_0(B)$, M_B, $(U-V)$, O/H and Ψ (solid curves) is shown as a function of redshift z, along with the $\pm 1\sigma$ values of the same quantities (inside dark shaded areas). There is little increase in $\langle R_B\rangle$ for $z < 1$ (induced mostly by low-mass discs), while $\langle\mu_0\rangle$ and $\langle\Psi\rangle$ decrease slightly at $z < 2$. Other average quantities ($\langle M_B\rangle, \langle U-V\rangle, \langle O/H\rangle$) increase constantly, from $z \sim 4$ to $z = 0$. In most cases, the corresponding values for the Milky Way (dotted curves) are larger than the average ones (because the latter are dominated by low-mass discs).

In fact, except for the case of R_B and Ψ, the Milky Way values are higher than the average ones by more than 1σ during most of the evolution. The Milky Way is a large spiral and its evolution is different from the average one not only quantitatively, but also qualitatively in some cases (e.g. in the case of M_B and μ_0 where the Milky Way values decline for $z < 2$ while the average ones continue to increase or remain constant).

At this point, we notice that most (but not all) semi-analytical models of galaxy evolution today use the Salpeter IMF (a power law with a unique slope -1.35 over the whole stellar mass range), which is flatter than the one used here. In Paper I we discussed at

length the reasons for our choice and the current observational evidence against a unique slope IMF. We also mentioned briefly the main differences resulting from its use, mainly the fact that it produces a larger effective yield of metals and a smaller number of stars of mass 1–2 $M_\odot$, which dominate the galactic luminosity at late times. As the effective yield of a stellar generation depends not only on the IMF but also on the individual stellar yields, which are still uncertain by at least a factor of 2 (see Prantzos 2000 and references therein), the former effect of the choice of the IMF cannot be tested against observations today. As for the latter, we

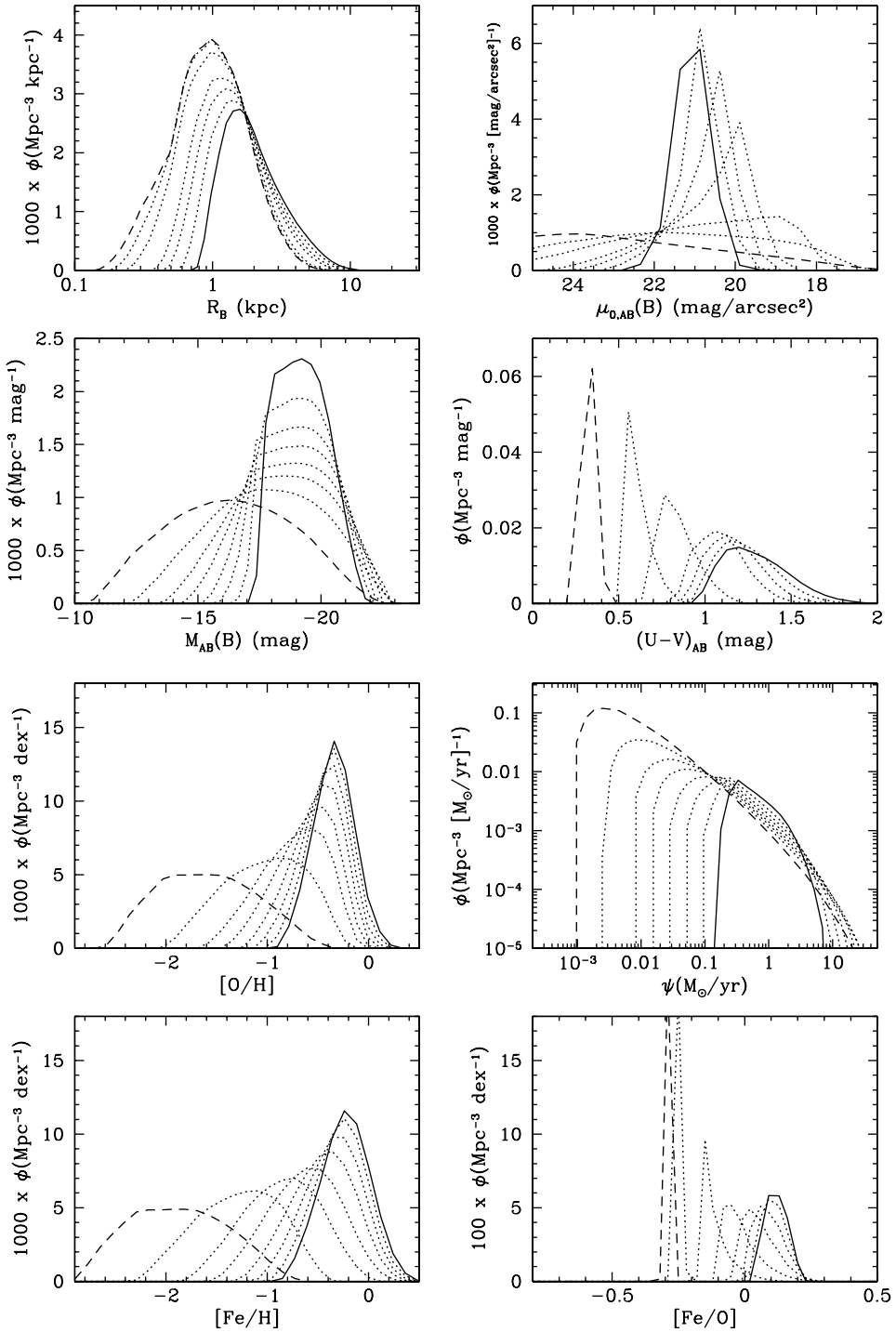

Figure 2. Evolution of the distribution functions $\phi(Q)$ of various output parameters Q of our models. Results are shown at different redshifts, starting with $z = 4.3$ (dashed curves), then $z = 2.8$, 1.7, 1.2, 0.7, 0.5, 0.2 (dotted curves) and $z = 0$ (solid curves). Top left: distribution of disc scalelength in the B-band R_B. Top right: distribution of central surface brightness in the B-band $\mu_{0,AB}(B)$. Second row left: distribution of disc rest-frame absolute magnitude in the B-band $M_{AB}(B)$. Second row right: distribution of disc colour $(U - V)_{AB}$. Third row left: distribution of disc average metallicity [O/H]. Third row right: distribution of star formation rate Ψ. Bottom left: distribution of disc average metallicity [Fe/H]. Bottom right: distribution of disc average abundance ratio [Fe/O]. Our models cover the range $80 < V_C(\mathrm{km\,s^{-1}}) < 360$ and represent high surface brightness discs today (with $\mu_0(B) < 22.5\,\mathrm{mag\,arcsec^{-2}}$), but some of them were low surface brightness discs in the past.

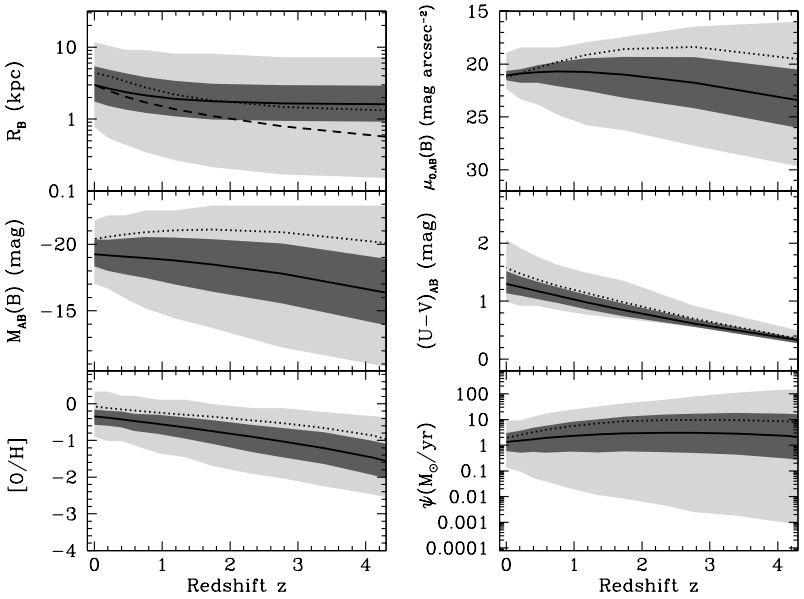

Figure 3. Evolution of several quantities computed with our models as a function of redshift: scalelength R_B (top left), B magnitude $M_{AB}(B)$ (middle left), average oxygen abundance (bottom left), central surface brightness $\mu_{0,AB}(B)$ (top right), colour index $(U-V)_{AB}$ (middle right) and star formation rate Ψ (bottom right). In all panels the solid curve indicates the average value of the probability distributions in Fig. 2, while the borders of the dark shaded area indicate the evolution of the corresponding $\pm 1\sigma$ values and the light shaded area represents the remaining discs. The dotted curves indicate the corresponding quantities for the Milky Way disc. The dashed curve in the upper left figure indicates the predictions of hierarchical models by Mao et al. (1998), according to which $R_B \propto (1+z)^{-1}$.

find that it results in differences of ~30 per cent in luminosity at late times, i.e. ~0.15 mag in the B band; this is also comparable to other theoretical uncertainties entering our calculation (neglect of late AGB phase in the adopted stellar tracks, crude treatment of dust etc.)

4 EVOLUTION UP TO $z = 1$: MODELS VERSUS OBSERVATIONS

In this section we compare our results to recent observations concerning the evolution of discs at moderate redshifts, for $z < 1$. A nice recent overview of the relevant observations can be found in Hammer (1999).

4.1 Large versus small discs

Lilly et al. (1998) used two-dimensional surface brightness profiles extracted from *HST* images of galaxies selected from the CFRS and LDSS redshift surveys to study the evolution of several properties of star-forming galaxies between $z = 0$ and $z = 1.3$. Their observations concern the disc scalelength R_B, magnitude $M_{AB}(B)$, central surface brightness $\mu_{AB,0}(B)$ and colour index $(U-V)_{AB}$.

The data of Lilly et al. (1998) concern galaxies of various inclinations, and are not corrected to the face-on case; however, those data do not show any trend with inclination. We checked that the scatter produced by varying the inclination in our models from 0° to 50° is smaller than the scatter obtained via the variation of the parameters V_C and λ. We thus present our results for galaxies seen face-on. The comparison of the data of Lilly et al. (1998) with our 'face-on' models serves merely to check whether the 'average' history of our models is compatible with the observational trends.

The data of Lilly et al. (1988) concern only large discs, with scalelengths $R_B > 4\,h_{50}^{-1}$ kpc. We selected then in our models discs satisfying this criterion and we plotted in Fig. 4 the results concerning the evolution of R_B, $\mu_0(B)$, M_B and $(U-A)_{AB}$ in a way similar to the one used in Fig. 3; this time, only the part of the distribution function of Fig. 2 concerning large discs is used to derive average and $\pm 1\sigma$ values, and results are shown only in the $z < 1.3$ range, where the measurements of Lilly et al. (1998) were made.

As can be seen in Fig. 4 (left top panel), the data show no evolution of R_B up to $z \sim 1$. The behaviour of our models is compatible with this trend, because most large discs are already formed at $z \sim 1$ and undergo very little increase in size afterwards. Note that our models do not reproduce the largest galaxies of the Lilly et al. (1998) sample (those with $R_B > 10$ kpc). Such discs are never obtained in our models and we consider that they are not representative of 'normal' spirals like those of the local sample of de Jong (1996) on which we based our model in Paper II. We notice that the Milky Way has a more rapid late evolution than an average disc: its R_B (*dotted curve* in Fig. 3) decreases by a factor of ~2, from ~4 kpc at $z = 0$ to ~2 kpc at $z \sim 1.2$. In this redshift range the Milky Way behaves almost as expected from the hierarchical scenario of Mao et al. (1998), i.e. with $R_B \propto (1+z)^{-1}$.

Observed B magnitudes (left bottom panel) exhibit some decline since $z \sim 1$. This is in qualitative agreement with our models and is related to the decrease of star formation with time in massive galaxies (Paper II). The range of M_B predicted by the models is also in fair agreement with the observed one. A comparison with Fig. 3 shows that the situation differs a lot from the case where all discs are taken into account: in that case, the average M_B increases lately, because of the late brightening of the numerous small discs.

There is also a slight decline of the observed central surface brightness of discs between $z = 0$ and $z = 1$ (right top panel), in agreement again with the evolution of our model $\phi[\mu_{0,AB}(B)]$ for large discs.

The right bottom panel of Fig. 4 shows the evolution of the $(U-V)_{AB}$ colour index. The data seem to indicate a strong

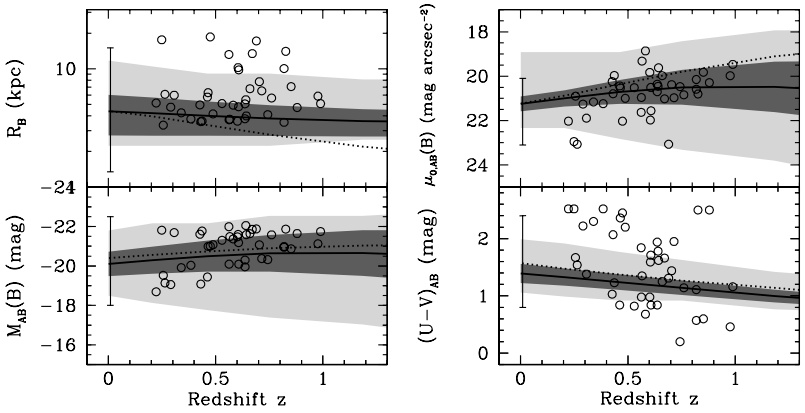

Figure 4. Evolution of scalelength R_B, magnitude $M_{AB}(B)$, central surface brightness $\mu_{0,AB}(B)$ and colour index $(U-V)_{AB}$ in the range $0 < z < 1.3$. The presentation of our results is similar to that of Fig. 3, but the average (solid curves) and $\pm 1\sigma$ values (borders of the shaded area) were calculated taking into account only the portion of the distribution function concerning large discs ($R_B > 4\,h_{50}^{-1}$ kpc). Observations of large discs by Lilly et al. (1998) are shown as circles. Observations of the local sample of de Jong (1996) are inside error bars. The Milky Way evolution is shown with dotted curves.

increase of that colour index with redshift (albeit with a large scatter). This is quite at odds with the results of our models, which predict a slow evolution in this redshift range. However, as noticed by Lilly et al. (1998) the colour of discs in the local sample of de Jong (1996) has a mean value of $(U-V)_{AB} \sim 1.5$, considerably smaller than their observations at moderate redshift (which suggest a mean value of 2 at $z \sim 0.3$). Notice that our models reproduce correctly colours at redshift $z = 0$, because they were constructed as to match local observations.

The local values of de Jong (1996), combined with the observations of Lilly et al. (1998) point towards little colour evolution on average, as in our models. However, the large scatter in the $(U-V)$ data cannot be explained by our histories of spiral galaxies. Brinchmann & Ellis (2000) notice that colour is a transient property. It could be affected by small episodes of interaction, or of enhancement of star formation, effects that are not taken into account in our models (which give an 'average' history of galaxies) and could perhaps explain part of the observed scatter.

The observations of Lilly et al. (1998) suggest a modest amount of evolution of large discs in the redshift range $0 < z < 1$, in agreement with the results of our models. This is also compatible with the conclusion of Brinchmann & Ellis (2000), who found that massive galaxies achieved the bulk of their star formation before $z \sim 1$.

Another conclusion of Lilly et al. (1998) is that the main evolutionary changes between $z = 1$ and $z = 0$ among spirals concern small (i.e. with half-light radii $R_{\rm Eff} < 5\,h_{50}^{-1}$ kpc) rather than large discs. Their fig. 17 illustrates the existence of small and bright discs at redshift $z \sim 1$, with no local counterparts. Our model also predicts a stronger evolution of properties among small galaxies than among large ones, and the existence of small and luminous spirals at high redshift.

This can be seen in Fig. 5, where we present the luminosity function $\phi(M_B)$ computed at three redshifts ($z = 0$ at the top, $z = 0.7$ in the middle, $z = 1.2$ at the bottom). The first column presents the results for all discs, the second column those for 'large' discs only ($R_B > 4\,h_{50}^{-1}$ kpc), and the third column those for 'small' discs ($R_B < 4\,h_{50}^{-1}$ kpc) The local luminosity function (all discs, $z = 0$, top left panel) is compared with Schechter functions determined for spiral galaxies of the APM survey (Loveday et al. 1992) and the SSRS2 survey (Marzke et al. 1998). Taking into account the facts that the determination of the luminosity function varies from sample to sample, that it is affected by the choice of cosmological parameters, and that we consider only models of face-on spiral galaxies, we think that the agreement of the computed luminosity function with the observationally derived ones is fairly good.

As already shown in Fig. 4, large discs were on average brighter in the past, at least up to $z \sim 1$. Fig. 5 reveals that they were also less numerous, because some of those had $R_B < 4\,h_{50}^{-1}$ kpc in the past. The important feature of Fig. 5, however, is that small discs (right panels) were both fainter and brighter in the past. A large number of small discs (comparable with their observed local population) were brighter by $\sim$2 mag on average in the past. In our models, those are moderately massive discs, the external parts of which were formed recently. At $z \sim 1$ they are already bright, but not large enough. This population of 'small' and bright discs at high redshift has no counterpart today and could well constitute the galactic population detected by Lilly et al. (1998). We further discuss this point at the end of Section 4.3.

4.2 The $R_{\rm d}$–$V_{\rm C}$ relationship

The variation of disc size, surface brightness, magnitude etc. with redshift can help to test theories of galaxy formation and evolution. Mao, Mo & White (1998) used data at low and high redshift to deduce that $R_{\rm d} \propto (1+z)^{-1}$, in agreement with hierarchical models of galaxy formation.

Before presenting our results and their comparison to observations, we notice that the *size* of a disc is usually measured by its exponential scalelength. But a disc can also grow by simply increasing its central surface brightness and keeping the same scalelength: it is difficult to claim that its 'size' remains constant in that case (indeed, its R_{25} radius increases). The use of scalelength to measure size may create some problems in that context.

With this caveat in mind, we proceed to a comparison between our models and observation, concerning the quantity $\mathrm{Q} = \log(R_B/V_{\rm C})$. The two histograms in the top left panel of Fig. 6 are adopted from Mao et al. (1998). One was computed for a local sample of discs (Courteau 1996, 1997; solid line), and the other for the high-redshift ($z < 1$) galaxies of Vogt et al. (1996, 1997; dotted line). The comparison of the two histograms shows that discs in the high-redshift sample are smaller for a given

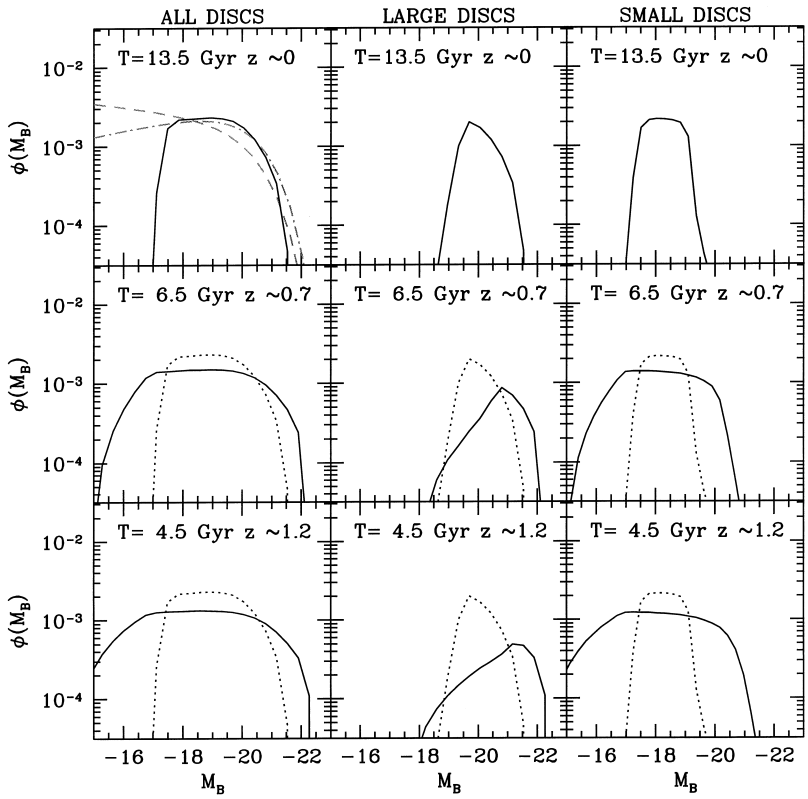

Figure 5. Evolution of the luminosity function of discs as a function of size, up to $z \sim 1.2$. The luminosity function for all discs is shown in the first column, while in the second and third columns we present the luminosity function of 'large' discs and 'small' discs, respectively. The limit between large and small discs is $R_B > 4\,h_{50}^{-1}$ kpc, adopted from Lilly et al. (1998). In the top panels, the functions are shown at redshift $z = 0$ (galactic age $T = 13.5$ Gyr), in the middle panels at redshift $z \sim 0.7$ ($T = 6.5$ Gyr) and in the bottom panels at $z \sim 1.2$ ($T = 4.5$ Gyr). The local ($z = 0$) functions of the top panels (solid curves) are repeated as dotted curves in the lower panels, in order to show the evolution of $\phi(M_B)$ between low and high redshifts. The local luminosity function for all discs of our models (top left panel) is compared with two Schechter-type fits to observational data (grey curves), obtained for spiral galaxies with the APM survey (Loveday et al. 1992) and the SSRS2 survey (Marzke et al. 1998). According to our models, large discs were brighter in the past, while small discs were both brighter and fainter than today.

velocity. In the bottom left panel we present our results for all discs. We also find that for a given V_C discs were smaller in the past, and to an extent slightly smaller than inferred from observations; in fact, as can be seen in Fig. 3, the mean value of our model R_B was smaller in the past, up to $z \sim 1$, but its rate of variation was closer to $(1+z)^{-0.5}$ than to $(1+z)^{-1}$.

These conclusions could be affected by various bias at high redshifts: for instance, the study of Lilly et al. (1998) presented in Section 3.2 deals only with large and bright discs, because fainter discs are not easily resolved. For this reason, we present in the right part of Fig. 6 the distribution of $Q = \log(R_B/V_C)$ for bright discs only ($M_B < -20$, top panel), and for large discs only ($R_B > 4\,h_{50}^{-1}$ kpc, bottom panel). In both cases, the position of the maximum of $\phi(Q)$ is clearly shifted to lower values at high z, but the shift is smaller in the case of large discs. Thus, we find that (R_B/V_C) should be always smaller on average at high z, but the value of the shift depends (albeit not very strongly) on the sample selection criteria.

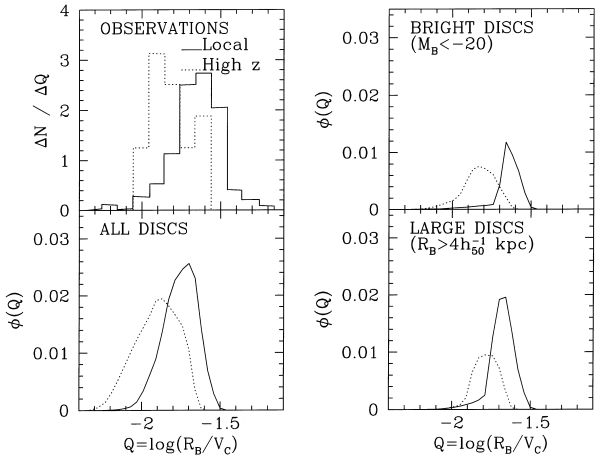

Figure 6. Evolution of the distribution of $Q = \log(R_B/V_C)$, where R_B is in kpc and V_C in km s^{-1}. Top left panel: histograms derived by Mao et al. (1998) for a local sample (Courteau 1996, 1997; solid), and for the high-redshift ($\langle z \rangle \sim 0.7$) sample of Vogt et al. (1996, 1997; dotted). The comparison of the two samples suggests that discs at high redshift were smaller for a given velocity. Bottom left panel: distribution computed with our models at redshift $z = 0$ (solid curve) and at redshift $z \sim 0.7$ (dotted). We find a trend similar to the observationally inferred one (albeit of slightly smaller magnitude), owing to the 'inside-out' formation of discs in our models. Top right panel: Same as bottom left panel, for bright discs only ($M_B < -20$). Bottom right panel: Same as bottom left panel, for large discs only ($R_B > 4\,h_{50}^{-1}$ kpc).

4.3 The R_d–M_B relationship

Mao et al. (1998) have also investigated the evolution of the magnitude–size relationship as a function of z. Fig. 7 (top left panel) shows the distribution of the quantity $Q = \log(R_B) + M_B/7.5$ that they obtained for a local sample (from Kent 1985) and for the high-redshift data of Schade et al. (1996). The latter

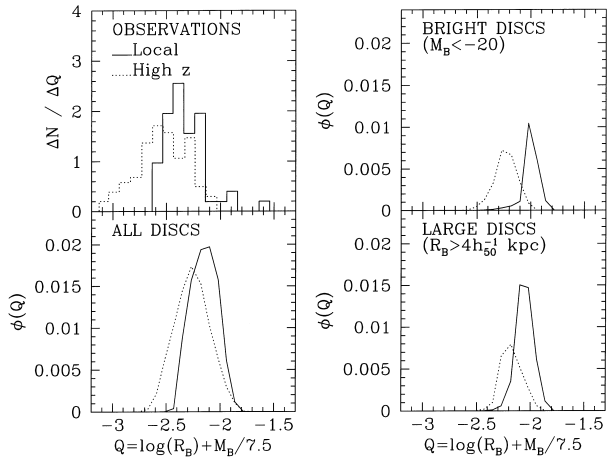

Figure 7. Evolution of the distribution of $Q = \log(R_B) + M_B/7.5$, where R_B is in kpc. Top left panel: histograms derived by Mao et al. (1998) for a local sample (Kent 1985, solid), and for the high-redshift ($\langle z \rangle \sim 0.7$) sample of Schade et al. (1996, dotted). The comparison of the two samples suggests that discs at high redshift were smaller for a given magnitude (or, equivalently, they were brighter for a given size). Bottom left panel: distribution computed with our models at redshift $z = 0$ (solid curve) and at redshift $z \sim 0.7$ (dotted). We find an effect compatible with the observationally inferred one. However, the observed high-z distribution is broader than ours. Top right panel: same as bottom left panel, for bright discs only ($M_B < -20$). Bottom right panel: same as bottom left panel, for large discs only ($R_B > 4\,h_{50}^{-1}$ kpc).

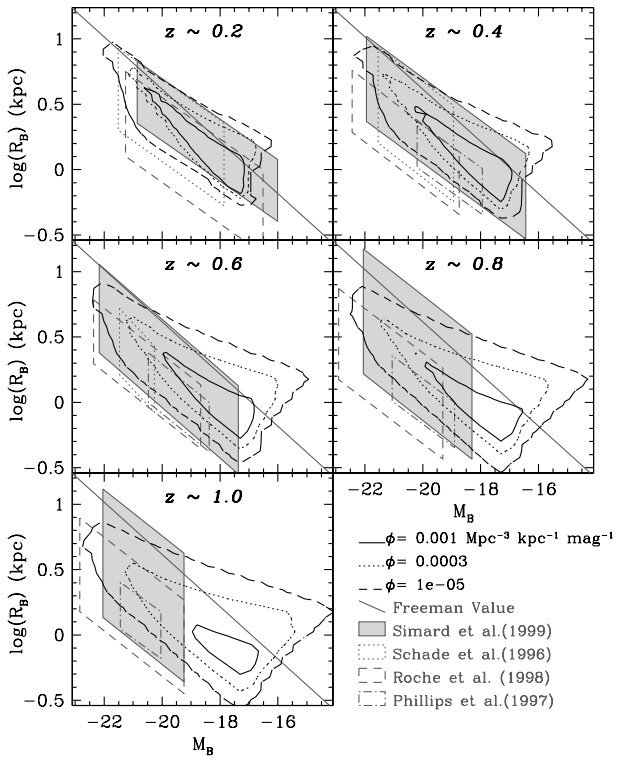

Figure 8. Disc scalelength R_B versus disc rest frame absolute magnitude M_B as a function of redshift z. The grey boxes indicate various observed samples, with the one of Simard et al. (1999) shaded; detection limits are displaced to lower magnitudes as one moves to higher redshifts. Our model results, convolved with the λ and V_C probability functions of Fig. 1, are shown as isodensity contours, with the largest number of discs included inside the solid curve. At high redshifts, only the brightest of our discs are present in the observational data. The grey diagonal line in all panels indicates the Freeman value of central surface brightness: $mu_{B,0} = 21.65$ mag arcsec^{-2} (Freeman 1970).

distribution is shifted with respect to the former one towards lower values of Q. From this comparison Mao et al. (1998) deduce that the size–magnitude relation must have evolved since $z \sim 1$, in the sense that discs of a given luminosity were smaller at early times (or, equivalently, discs of a given size were brighter). The distributions of this same quantity in our models are shown in the left bottom panel, for redshifts $z = 0$ and 0.7, respectively. We also obtain a shift between the two, compatible with the one inferred from the observations. However, our distributions (especially the high-redshift one) are narrower than the observed ones and slightly shifted to larger Q values. The reason for this small discrepancy may be the fact that we consider discs with $V_C > 80\,\mathrm{km\,s^{-1}}$, i.e. slightly brighter than the lower limit considered in the observed samples.

The right panels of Fig. 7 show the same quantity for bright discs (top) and large discs (bottom). We find again the same effect, i.e. a shift of parameter Q towards higher values with time. Selection criteria do not then affect this result, namely that discs of a given size were brighter in the past. In fact, this is another way of presenting the result of Fig. 4, showing that large discs were slightly brighter in the past.

More recently, Simard et al. (1999) analysed 190 field galaxies of the DEEP survey in order to determine the magnitude–size relationship of discs in several redshift bins, up to $z \sim 1.1$. Their survey is statistically complete for magnitudes $I_{814} < 23.5$. The envelope of their observations at a given redshift (taken from their paper) is shown in Fig. 8 along with a few other magnitude–size samples (Schade et al. 1996; Phillips et al. 1997; Roche et al. 1998), including the one of Schade et al. (1996) that was discussed in Fig. 7. The solid diagonal line in each panel is the locus of the local Freeman relation $\mu_{0B} = 21.65$ mag arcsec^{-2} (Freeman 1970). To a first approximation, the data follow this relation at all redshifts, with some increase of the size dispersion at a given magnitude. Also, in the highest redshift bins, the average μ_{0B} value of the observed samples is higher than the Freeman value. This is another way of presenting the results of Fig. 7, namely that at high z discs of a given magnitude were smaller, on average.

Our models of R_B versus M_B are also plotted as a function of redshift in the various panels of Fig. 8. We show the isodensity contours, as indicated in the bottom right panel of the figure. Our results compare fairly well to the observations of Simard et al. (1999) in the redshifts $z \sim 0.2$ and $z \sim 0.4$. At higher redshifts, the dispersion of R_B for a given M_B increases, while the average R_B value decreases, both in agreement with the observations. In fact, in the highest redshift bins, the largest part of our model discs is fainter than the cut-off magnitude M_B of the Simard et al. (1999) survey; only our brightest discs (the luminous 'tip of the iceberg') are seen in the observations, and their behaviour is entirely compatible with the data. The size dispersion of our discs is due to the effect of the spin parameter λ on their structure and evolution (through the adopted scaling relations and the SFR and infall prescriptions, see Section 2.2). For all λ values, massive discs attain their final size early on (before $z \sim 1$) and evolve little at late times, as discussed in Section 4.1. But, depending on the λ value, low-mass discs may have very different histories: compact ones (low λ) evolve rapidly, i.e. before $z \sim 1$, while extended ones (large λ) evolve more slowly. This explains the large dispersion in the R_B values of faint discs at high redshift.

Simard et al. (1999) draw attention to the fact that the apparent

increase of mean surface brightness with z in their data may be entirely the result of selection effects; if the survey selection functions are used to correct the surface brightness distributions in the different redshift bins, no significant evolution is found in their data up to $z \sim 1$ for discs brighter than $M_B = -19$.

This is at odds with the results of our models, which generically predict an increase of the mean surface brightness with redshift up to $z \sim 1$. This increase is due to the fact that most of our discs form their central regions long before $z \sim 1$; the SFR and the corresponding surface brightness of those regions can only decline at late times, i.e. increase with redshift. Notice that the situation is different for $z > 1$: bright discs exhibit the same trend up to $z \sim 2$ (because the evolution of their central regions is completed earlier than that), while faint galaxies have mean surface brightness declining with z. According to our senario, they still form their inner regions in the $z = 1$–2 redshift range.

Nine galaxies at $z > 0.9$ of the Simard et al. (1999) sample occupy a region of the $R_B - M_B$ plane rarely populated by local galaxies, i.e. they are bright and relatively compact. In our senario, such high surface brightness discs do exist at $z \sim 1$: they are high V_C and low λ discs that have completed their evolution earlier than $z \sim 1$ and became progressively fainter at late times (by $\sim$1 mag in M_B in the past $\sim$6–7 Gyr).

4.4 Tully–Fisher relation

The Tully–Fisher (TF) relation is a strong correlation exhibited by the whole population of disc galaxies. It relates their luminosity L or magnitude M and their circular velocity V_C, through $L \propto V_C^{a/2.5}$ or $M = -a[\log(2V_C) - 2.5] + b$. The exact slope of the relation and its zero-point are still the subject of considerable debate (see e.g. Giovanelli et al. 1997).

In Paper II we presented a detailed comparison of our model results to local ($z \sim 0$) TF relations obtained by different groups in the I and B bands. We noticed that in the I band (which presumably reflects better the underlying stellar population) the TF slopes of different groups differ by more than $\sim$20 per cent (i.e. from $a = 6.80$ in Mathewson, Ford & Buchhorn 1992 to 8.17 in Tully et al. 1998).

Our results are in much better agreement with the data of Han & Mould (the corresponding TF relationship is given in Willick et al. 1996) or Mathewson et al. (1992), concerning field spirals, than with those of Tully et al. (1998) or Giovanelli et al. (1997), which concern spirals in clusters. We notice that our models correspond better to the former case than to the latter, because star formation in cluster galaxies may be affected by tidal interactions which are not taken into account in our SFR prescription.

In the B band, the available local TF relation of Tully et al. (1998) again concerns spirals in clusters. Our model B-band TF relation is slightly flatter than the observed one, but in view of the uncertainties and the caveats mentioned in the previous paragraphs, we do not think that this a serious drawback of the models. We note that other models (e.g. Mo et al. 1998; Heavens and Jimenez 1999; Bouwens & Silk 2000) apparently reproduce better the local B-band TF relation. However, the mass-to-light ratio M/L in those models is either taken as constant or is adjusted as a function of V_C in order to reproduce the TF relation. Our own M/L versus V_C relation (presented in fig. 8 of Paper II) is computed from the fully self-consistent chemo-spectrophotometric evolution models, which reproduce all the main properties of local discs without any adjustment except for the initial scalings (see Section 2.2 and Paper II).

Using spectroscopic observations of the Keck telescope and high-resolution images from the *Hubble Deep Field*, Vogt et al. (1996, 1997) determined a TF relation for 16 galaxies lying between redshifts $z = 0.15$ and 1 in the rest-frame B-band. They find no obvious change in the shape or slope of the TF relation with respect to the local one. Assuming the same slope, they derive a modest brightening of 0.36 ± 0.13 mag between redshifts $z \sim 0$ and 1. Their data, split in two redshift bins ($0.2 < z < 0.6$ and $0.6 < z < 1$, respectively) are shown in Fig. 9.

We also present in Fig. 9 the TF relationship computed with our grid of models at four galactic ages, corresponding to $z \sim 0$, 0.4, 0.8 and 1.2, respectively (from top to bottom). In the top panel, results are compared with the local B-band observations of Tully et al. (1998). In the second and third panels, our model TF relations are compared with the data of Vogt et al. (1996, 1997). Our results are certainly compatible with the data, but in view of the large error bars and selection effects (only the brightest galaxies are detected in the $z \sim 0.8$ bin) no strong conclusions can be drawn. It is clear, though, that our models predict a steepening of the TF relation in the past, because massive discs were brighter, on average, than today, while low-mass discs were fainter. This steepening with respect to the local slope is small and difficult to detect at $z \sim 0.4$ and more important at higher redshifts. We also notice that at high redshifts the dispersion in luminosity becomes larger for the fainter

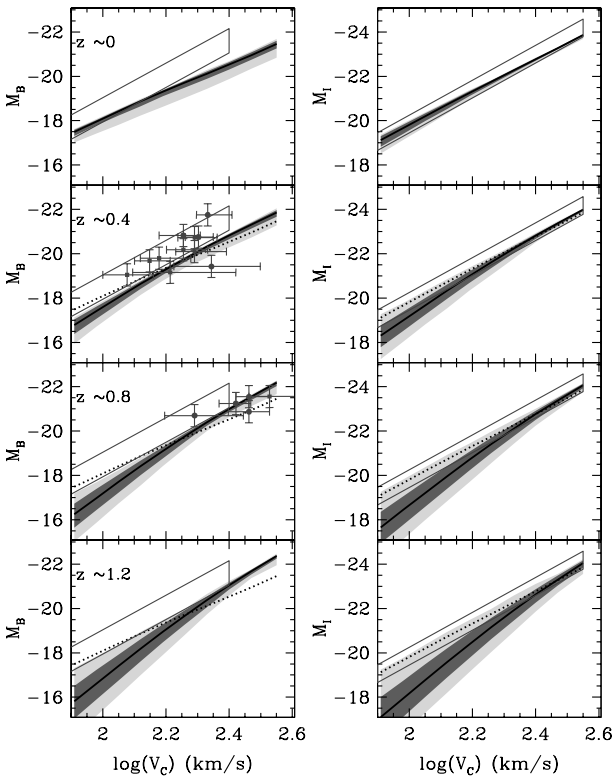

Figure 9. Evolution of the Tully–Fisher relation as a function of redshift z (from top to bottom) in the B and I bands (left and right, respectively). The average relationship obtained with our models is shown as solid curve, among $\pm 1\sigma$ values (dark shaded area) and all remaining discs (light shaded area); in the bottom three panels, the dotted curve is the average model TF relation of the top panel ($z = 0$), allowing to measure the evolution. Boxes in all the left panels represent the observed local TF relation in the B band (Tully et al. 1998), while boxes in all the right panels show the local TF relation in the I band (Mathewson et al. 1996). Data at high redshift in the left panels are from Vogt et al. (1996, 1997).

discs. In both cases, observations of faint galaxies ($M_B > -18$) would be required to establish the behaviour of the TF relation at high redshift.

5 EVOLUTION AT REDSHIFT $z > 1$

5.1 Scalelength distributions

The size–luminosity relation at redshifts $z > 1$ has been recently investigated by Giallongo et al. (2000). They used data from the *Hubble Deep Field* North, where morphological information is available for all galaxies up to apparent magnitude $I \sim 26$. Using colour-estimated redshifts and assuming exponential scalelengths, they derived absolute blue magnitudes M_B and disc scalengths R_d as a function of redshift. They compared these data, concerning the redshift range $1 < z < 3.5$, with those of the ESO–NTT deep field, concerning the redshift range $0.4 < z < 1$ (Fontana et al. 1999). The results of their study appear in Fig. 10 (histograms) for 'bright' and 'faint' discs (upper and lower panels, respectively). Comparing these with predictions of 'standard' semi-analytical models, including merging histories for dark haloes, Giallongo et al. (2000) found a significant excess (by a factor of ~3) in redshift ranges of both bright and small discs (i.e. discs with $R_d <$ 2 kpc in the low-redshift range and with $R_d < 1.5$ kpc in the high-redshift range); they also found a smaller excess (by ~50 per cent) of 'faint' discs in both redshift ranges.

Our results are also plotted in Fig. 10. In each panel, *dotted* and *dashed* curves indicate scalelength distributions obtained at the two extremes of the corresponding redshift range. When adding the model distributions of the upper and lower panels at a given z one obtains the total distribution of R_B for that z, shown in Fig. 2. We notice that the observed and model distributions are normalized differently (corresponding scales are indicated on the left and right axis of each panel), but the comparison of their shapes allows us to draw some interesting conclusions.

In the low-redshift range (left panels), our model distributions evolve very little between $z = 1$ and 0.4, with both 'bright' and 'faint' discs becoming larger with time. In both cases, distributions at $z = 1$ compare slightly better with the data than distributions at $z = 0.4$. The overall agreement with the data is excellent. We find no deficiency of small discs (either bright or faint ones), in contrast to Giallongo et al. (2000). We notice that we always use the probability distributions F_V and F_λ of Fig. 1, assuming no merging. This assumption turns out to be crucial for the agreement of models with the data. Indeed, taken at face value, the results in the left panel of Fig. 10 imply that the adopted prescriptions for the scaling relations, infall, SFR, F_V and F_λ are sufficient to produce discs with the correct distributions of scalelengths at intermediate redshifts.

In the high-redshift range (right panels of Fig. 10) we also find little evolution and excellent agreement with observations for the 'faint' discs ($M_B > -20$). We notice that, by construction, our models predict little early evolution for discs of low-mass and luminosity. For 'bright' discs, we find significant evolution in the R_B distribution, in the sense that this distribution is significantly shifted to larger and more numerous discs when the redshift decreases from $z = 3.5$ to $z = 1$: in that redshift range a large number of initially small and 'faint' discs (belonging to the lower right panel of Fig. 10 at $z = 3.5$) become brighter and larger at $z = 1$ (and 'migrate' to the upper panel), owing to the adopted inside-out formation scheme. However, none of the two model distributions compares well with the observed histogram, and this will obviously be true for any other model distribution at redshift $1 < z < 3.5$: we therefore find (as Giallongo et al. 2000) a serious deficiency (factor ~3) of small and bright discs at high redshift. We notice, however, that this is the only discrepancy of our models with respect to the observations, while Giallongo et al. (2000) found discrepancies in all four panels of Fig. 10.

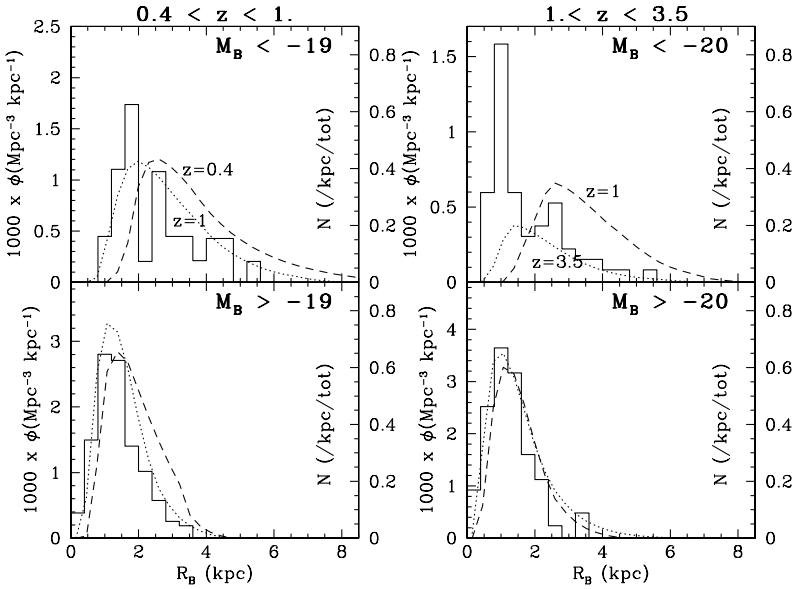

Figure 10. Distribution functions of the scalelength in the B-band R_B in two different redshift ranges: $0.4 < z < 1$. (left) and $1. < z < 3.5$ (right), respectively. In both redshift ranges, distributions concern 'bright' discs (upper panels) and 'faint' discs (lower panels), respectively; notice that the magnitude limits are different in the two cases ($M_B = -19$ on the left and $M_B = -20$ on the right). Observed distributions (histograms) are from the surveys of the ESO–NTT deep field at low z and of the *Hubble Deep Field* at high z (Giallongo et al. 2000); the corresponding scales on the vertical axis are displayed on the right of each panel. In each panel we show two model distributions (in dotted and dashed curves, respectively) corresponding to the two extremes of the corresponding redshift range, i.e. at $z = 0.4$ and 1 in the left panels and at $z = 1$ and 3.5 in the right panels, respectively. Our model distributions are not normalized to the observed ones and the corresponding scales are displayed on the left of the vertical axes.

The deficiency of our models concerns bright and small discs, i.e. discs with high surface brightness. Selection effects may play some role in that case, because they obviously favour the detection of such discs at the expense of more extended ones having lower surface brightness. If there is no selection bias in the data, then it is the first hint that our models (based on the simple prescriptions of Section 2) may have some difficulties in reproducing observables of the high-redshift Universe. In fact, our models are 'calibrated' on the Milky Way disc and the infall time-scale adjusted so as to reproduce all major observables of discs in the local Universe (Papers II, III and IV). The dicrepancy encountered in Fig. 10 may imply that mergers between small discs (not taken into account here) did play some role in that redshift range: such mergers would affect only a small fraction of the population of the lower right panel of Fig. 10, but would contribute significantly in populating the deficient part of the curves in the upper right panel.

5.2 Abundance gradients versus scalelengths

In Paper III of this series (Prantzos & Boissier 2000a) we showed that a remarkable correlation exists between the abundance gradient of a disc (expressed in dex kpc^{-1}) and its scalelength R_B: small discs have large (in absolute value) abundance gradients and vice versa. This is easy to understand qualitatively, because abundance gradients are created by radially varying quantities, like the SFR $\Psi \propto R^{-1}$ adopted here. In a small disc (say, $R_B = 2$ kpc), such quantities vary significantly between regions which are only 1 kpc distant from each other; a large abundance gradient is obtained in that case. In a large disc (say $R_B = 6$ kpc) regions separated by 1 kpc have quite similar SFR; such discs cannot develop important abundance gradients, in dex kpc^{-1}.

Although intuitively obvious, this property has never been properly emphasized before. In Paper III it was shown that there is a unique relation between $\mathrm{d}\log(\mathrm{O/H})/\mathrm{d}R$ and $1/R_B$ for all discs. This relation is found in observed nearby spirals and is fairly well reproduced by our models of discs at $z \sim 0$, as can be seen on the upper left panel of Fig. 11. The importance of that correlation is obvious: the abundance gradient can be derived if the disc scalelength is known and vice versa.

In this section we explore whether this correlation is valid at higher redshifts. In Fig. 11 we plot the relation of $\mathrm{d}\log(\mathrm{O/H})/\mathrm{d}R$ versus $1/R_B$ for our model discs at redshifts $z = 0$ (where they compare quite favourably with observations), $z = 1.5$ and $z = 3$. At all redshifts we find the relation obtained locally. The 'homologous evolution' of spirals, invoked by Garnett et al. (1997) for local discs, is also found in the high-redshift Universe.

In the lower panel of Fig. 11 we present then the quantity $\mathrm{d}\log(\mathrm{O/H})/\mathrm{d}R_B$ of our models (i.e. the abundance gradient expressed in dex R_B^{-1}, instead of dex kpc^{-1}). We plot this quantity, weighted by the probability functions F_V and F_λ, as a function of redshift. It can be seen that during most of the history of the Universe, this quantity remains ~constant, at a value of $\mathrm{d}\log(\mathrm{O/H})/\mathrm{d}R_B \sim -0.20$ dex$/R_B^{-1}$; only at very late times does this quantity increases slightly (in absolute value), having been dominated by the numerous small discs that evolve considerably in the $z \sim 0. - 0.5$ range. For that same reason, the dispersion around

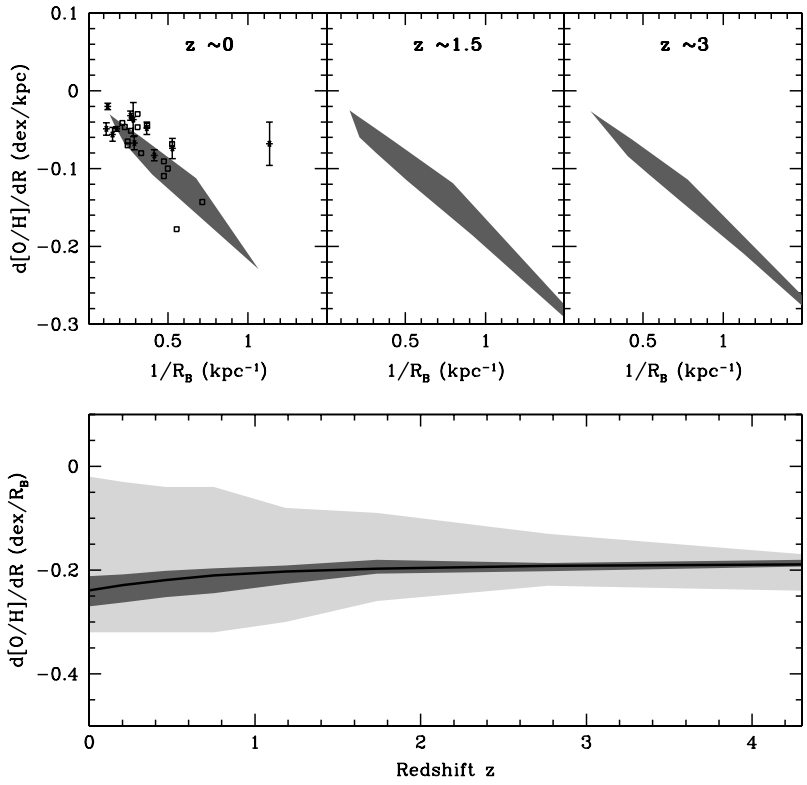

Figure 11. Upper panels: relation between the abundance gradient of oxygen $\mathrm{d}\log(\mathrm{O/H})/\mathrm{d}R$ and the inverse of the scalelength R_B as a function of redshift. The relationship found for local discs in Paper III (Prantzos & Boissier 2000a) is supported by observations. Data at $z \sim 0$ from Garnett et al. 1997 (open squares) and van Zee et al. 1998 (filled circles with error bars); the one discrepant point of van Zee et al. (1998) concerns an extremely small and low surface brightness disc. We find a similar anticorrelation also at higher redshifts; discs evolve 'homologously'. Lower panel: the abundance gradient of our models, expressed in dex R_B^{-1} and weighted by the probability functions F_V and F_λ of Fig. 2, is plotted as a function of redshift (Solid curve: average value; dark shaded area: $\pm 1\sigma$ values; light shaded area: all other discs).

this value increases at low z. Both the stability of the relation of $\mathrm{d}\log(\mathrm{O/H})/\mathrm{d}R$ versus $1/R_B$ and the decrease in the dispersion of $\mathrm{d}\log(\mathrm{O/H})/\mathrm{d}R_B$ with redshift are novel and important predictions of our model. If true, they will allow us to infer something about the chemistry of high-redshift discs from their morphology.

At this point, we notice that damped Lyman α systems (DLAs) may be (proto-)galactic discs such as those considered here: in a previous paper (Prantzos & Boissier 2000a) we have shown that, when observational bias is taken into account, the observations of Zn abundance in such systems as a function of their redshift ($0.5 < z < 3.5$) are nicely explained by our models. The apparent 'no chemical evolution' picture suggested by the observations of those systems (e.g. Pettini et al. 1999) is quite compatible with our understanding of the chemical evolution of discs.

6 SUMMARY

In this paper we explore the implications of our disc galaxy models for the high-redshift Universe. Our models (presented in detail in Papers I, II, III and IV) are 'calibrated' on the Milky Way, utilize simple prescriptions for the radial variation of the SFR and infall rate and simple scaling relations (involving rotational velocity V_C and spin parameter λ) and reproduce all major observables concerning discs in the local Universe. A crucial ingredient for the success of our models is the assumption that massive discs form the bulk of their stars earlier than their low-mass counterparts.

We assume here that the probability functions F_V and F_λ of the two main parameters of our models are independent and do not evolve in time, i.e. we assume that mergers never play a significant role in the overall evolution of disc galaxies. We follow then the evolution of the distribution functions of various quantities and we compare the results with available observations concerning discs at high redshifts. Our results are summarized as follows.

(i) Most large discs ($R_B > 4\,h_{50}^{-1}$ kpc) have basically completed their evolution already by $z \sim 1$. Subsequently, they evolve at ~constant scalelength, while their luminosity and central surface brightness decline (Section 4.1). These features of our models are in quantitative agreement with observations of the CFH survey (Lilly et al. 1998). Our models also predict a mild evolution of $U - V$ colour of large discs in that redshift range, while the Lilly et al. (1998) data suggest a slightly stronger evolution; but their data, extrapolated to $z \sim 0$, are in disagreement with the local values derived by de Jong (1996), while our models reproduce fairly well the observations of the local sample. As $U - V$ colours can be strongly affected by 'transient' phenomena (e.g. short 'bursts' of star formation), we do not think that this discrepancy is a real problem for the models.

(ii) Because of the 'inside-out' formation scheme of discs adopted in our models, we predict that discs were, on average, smaller in the past for a given rotational velocity V_C or for a given magnitude M_B. Both results are in qualitative agreement with recent samples of discs at redshifts up to $z \sim 1$ (Sections 4.2 and 4.3). Our models reproduce fairly well the data of Simard et al. (1999) on the R_B versus M_B relation as a function of redshift, up to $z \sim 1$. In particular, our models produce some compact and bright discs that Simmard et al. (1999) find at $z \sim 1$ and which have no counterparts in the local Universe (Section 4.3).

(iii) We find that the Tully–Fisher relation was steeper in the past, with massive discs being, on average, brighter, and low-mass discs fainter than today. Our models are in agreement with observations of the TF relation in the B band obtained by Vogt et al. (1997) at intermediate redshifts ($z \sim 0.4$ and 0.8), taking into account their error bars (Section 4.4). However, these data are insufficient to probe the evolution of the TF relation, which requires data on fainter discs (down to $M_B \sim -18$ in that redshift range).

(iv) Our models reproduce fairly well the distribution of disc scalelengths of the ESO–NTT survey, concerning both bright and faint discs in the 0.4–1 redshift range (Section 5.1). They also reproduce well the scalelength distribution of faint discs in the 1–3.5 redshift range obtained in the *Hubble Deep Field* (Giallongo et al. 2000). In contrast, we fail to reproduce the corresponding distribution of bright discs in that same redshift range: our models show a defficiency of small ($R_B \sim 1$ kpc) and bright ($M_B < -20$) discs with respect to the *Hubble Deep Field* data. If this discrepancy is not explained in terms of selection effects (favouring the detection of those high surface brightness discs) it could be a strong indication that merging of small discs indeed played an important role in that redshift range.

(v) The anticorrelation between the abundance gradient $\mathrm{d}\log(\mathrm{O/H})/\mathrm{d}R$ (expressed in dex kpc^{-1}) and the scalelength R_B that we found in Paper III for local discs is found also to be valid at higher redshifts (Section 5.2). We find that the abundance gradient of discs, expressed in dex R_B^{-1}, varies very little with redshift and presents a smaller dispersion at high redshifts. These findings establish a powerful link between the optical morphology and the chemical properties of disc galaxies, valid in both the local and the distant Universe.

In summary, we explored the consequences of our 'backwards' model of disc galaxy evolution for the high-redshift Universe. We found no serious discrepancies with currently available data up to redshift $z = 1$. At higher redshifts, we find hints that the model may require some modifications, provided that currently available data are not affected by selection biases.

REFERENCES

Avila-Reese V., Firmani C., 2000, RevMexAA, 36, 23
Boissier S., Prantzos N., 1999, MNRAS, 307, 857 (Paper I)
Boissier S., Prantzos N., 2000, MNRAS, 312, 398 (Paper II)
Boissier S., Boselli A., Prantzos N., Gavazzi G., 2001, MNRAS, 321, 733 (Paper IV)
Boselli A., Gavazzi G., Donas J., Scodeggio M., 2000, AJ, 121, 753
Bouwens R., Silk J., 2001, ApJ, in press (astro-ph/0002133)
Bouwens L., Cayon L., Silk J., 1997, ApJ, 489, L21
Brinchmann J., Ellis R., 2000, ApJL, in press (astro-ph/0005120)
Calzetti D., Kinney A., Storchi-Bergmann T., 1994, ApJ, 429, 582
Cayon L., Silk J., Charlot S., 1996, ApJ, 467, L53
Charbonnel C., Meynet G., Maeder A., Schaerer D., 1996, A&AS, 115, 339
Chiappini C., Matteucci F., Gratton R., 1997, ApJ, 477, 765
Courteau S., 1996, ApJS, 103, 363
Courteau S., 1997, AJ, 114, 2402
deJong R., 1996, A&AS, 118, 557
Ferrini F., Molla A., Pardi M., Diaz A., 1994, ApJ, 427, 745
Firmani C., Avila-Reese V., 2000, MNRAS, 315, 457
Fontana A., Menci N., D'Odorico S., Giallongo E., Poli F., Cristiani S., Moorwood A., Saracco P., 1999, MNRAS, 310, L27
Freeman K., 1970, ApJ, 160, 811
Garnett D., Shields G., Skillman E., Sagan S., Dufour R., 1997, ApJ, 489, 63
Giallongo E., Menci N., Poli F., D'Odorico S., Fontana A., 2000, ApJ, 530, L73
Giovanelli R., Haynes M., Da Costa L., Freudling W., Salzer J., Wegner G., 1997, ApJ, 477, L1

Gonzalez A., Williams K., Bullock J., Kolatt T., Primack J., 2000, ApJ, 528, 145
Guiderdoni B., Hivon E., Bouchet F., Maffei B., 1998, MNRAS, 295, 877
Hammer F., 1999, in Hammer F., Thuan T.X.T., Cayatte V., Guiderdoni B., Tran Than Van J., eds, Proc. XIXth Rencontres de Moriond. Editions Frontières, Paris, p. 211
Heavens A., Jimenez R., 1999, MNRAS, 305, 770
Jimenez R., Padoan P., Matteucci F., Heavens A., 1998, MNRAS, 299, 123
Kent S. M., 1985, ApJS, 59, 115
Kroupa P., Tout C., Gilmore G., 1993, MNRAS, 262, 545
Lejeune T., Cuisinier F., Busser R., 1997, A&AS, 125, 229
Lilly S. et al., 1998, ApJ, 500, 75
Loveday J., Peterson B. A., Efstathiou G., Maddox S. J., 1992, ApJ, 390, 338
Mao S., Mo H., White S., 1998, MNRAS, 297, L71
Marzke R., da Costa L., Pellegrini P., Willmer C., Geller M. J., 1998, ApJ, 503, 617
Mathewson D., Ford V., Buchhorn M., 1992, ApJS, 81, 413
Matteucci F., Greggio L., 1986, A&A, 154, 279
Mo H., Mao S., White S., 1998, MNRAS, 295, 319
Pettini S., Ellison S., Steidel C., Bowen D., 1999, ApJ, 510, 576
Phillips A., Guzman R., Gallego J., Koo D., Lowenthal J., Vogt N., Faber S., Illingworth G., 1997, ApJ, 489, 543
Prantzos N., 2000, New Astron. Rev., 44, 303
Prantzos N., Aubert O., 1995, A&A, 302, 69
Prantzos N., Boissier S., 2000a, MNRAS, 313, 338 (Paper III)
Prantzos N., Boissier S., 2000b, MNRAS, 315, 82
Prantzos N., Silk J., 1998, ApJ, 507, 229
Renzini A., Voli M., 1981, A&A, 94, 175
Roche N., Ratnatunga K., Griffiths R. E., Im M., Naim A., 1998, MNRAS, 293, 157
Schade D., Carlberg R., Yee H., Lopez-Cruz O., Ellingson E., 1996, ApJ, 465, L103
Schaller G., Schaerer D., Meynet G., Maeder A., 1992, A&AS, 96, 269
Simard L. et al., 1999, ApJ, 519, 563
Steinmetz M., Navarro J., 1999, ApJ, 513, 555
Tinsley B., 1980, Fundam. of Cosmic Phys., 5, 287
Tully R., Pierce M., Huang J., Saunders W., Verheijen M., Witchalls P., 1998, AJ, 115, 2264
van den Bosch F. C., 1998, ApJ, 507, 601
van Zee L., Salzer J., Haynes M., O'Donoghue A., Balonek T., 1998, AJ, 116, 2805
Vogt N., Forbes D., Phillips A., Gronwall C., Faber S., Illingworth G., Koo D., 1996, ApJ, 465, L15
Vogt N. et al., 1997, ApJ, 479, L121
Willick J., Courteau S., Faber S., Burstein D., Dekel A., Kolatt T., 1996, ApJ, 457, 460
Woosley S., Weaver T., 1995, ApJS, 101, 181
Wyse R., Silk J., 1989, ApJ, 339, 700

This paper has been typeset from a TEX/LATEX file prepared by the author.